Current Sheet Structure in an Inductive-Impulsive Plasma Accelerator

C. L. DAILEY*
TRW Systems Group, Redondo Beach, Calif.
AND
R. H. LOVBERG†
University of California at San Diego, La Jolla, Calif.

Probe and laser light-scattering measurements of electron density have been made in the current sheet of a pulsed inductive accelerator. The discharge consists of a thin flat disk of pure j_θ current. The only current carriers are electrons. The gas is ionized and swept up into a 4 mm thick current sheet. Ions are accelerated by an axial E field, ahead of the mass layer, produced both by electron current and negative electron pressure gradient. This field nearly vanishes at the rear of the mass layer where $j \times B$ force balances the positive electron pressure gradient.

Introduction

THIS report presents the results of an experimental investigation of the physical processes within the current sheet of an impulsive plasma accelerator. An inductive device having a 20 cm diam, flat, spiral coil was used in order to separate the properties of the sheet from effects peculiar to a given experimental configuration, such as electrode sheaths, nonuniform conditions over the sheet area, etc.

For more than ten years, a variety of pulsed plasma devices have been studied experimenally in an effort to improve their usefulness for different purposes, to describe their operation and to understand the impulsive plasma current sheet. Included in this category are such geometries as coaxial plasma guns, conical guns, and pinches, both inductive (θ-pinch) and series connected (Z-pinch).

Experiments done in 1962 on a parallel-plate accelerator raised questions concerning the partitioning of current between electrons and ions in impulsive "snowplow" current sheets.[1] In that device it was observed that the electrostatic space-charge field, normally present in a sheet dominated by electron current, was nearly absent (when hydrogen was being accelerated). This result seemed to imply the existence of a major ion current component, and led to the formulation of a model in which the process of ionization of neutrals being overtaken by the current sheet quite naturally resulted in ion current flow.

This concept not only explained some of the current sheet features observed in accelerators employing electrodes, but seemed to apply equally well to the inductive type of accelerator.[2] However, in the latter case, momentum conservation parallel to the ion current required a net torque about the accelerator axis that did not seem to be possible in that geometry. Others have observed a rotation of the plasma in a θ-pinch.[3] It is argued that a radial component of current can occur as a result of electrons drifting to the wall along magnetic field lines and that this torque acts during the radial acceleration period.[4] We have looked for current and magnetic field components that would accompany such a torque mechanism in our flat spiral coil accelerator and have concluded that, for that geometry, such a mechanism is not present.[5]

Experiments were carried out in a θ-pinch for the specific purpose of investigating current partition.[6] It was operated without bias field or preionization and the second half-cycle was used for the measurements. The general Ohm's Law relation was used to obtain tangential (θ) velocity of the plasma (ions) in terms of plasma density, current density and electric and magnetic fields. A schlieren technique was used for the density measurement. The results did not indicate a uniformly rotating plasma, either for nitrogen or hydrogen. An important result of the hydrogen experiment was the appearance of a substantial radial electric field in the θ-pinch, unlike the very small axial field found in the parallel plate accelerator. This seemed to support the idea that ion current could appear in an electrode device but not in an inductive one.

With this result in hand it seemed desirable to make a similar analysis of the pulsed inductive accelerator (flat, spiral coil) using a Stark broadening measurement of density. The results of this set of measurements indicated that some of the current was carried by ions.[7] However, the ion current distribution was qualitatively different from that inferred earlier from collisionless ion trajectory calculations. A strong splitting of the current sheet into two parts was found, whereas, the earlier measurement had shown a secondary hump that was thought to be due to ion current following an electron current layer at the front of the sheet.

There has been a theoretical indication that pulsed operation might produce ion current. Spitzer discusses an idealized case of a fully ionized plasma in a uniform B field to which a perpendicular E field is suddenly applied.[8] By neglecting changes in E and B that would result from the subsequent current, he finds an ion current in the E field direction that is equal to the electron current component at a time

$$t = 1/(\omega\tau)_e\,\omega_i \tag{1}$$

where τ is the electron collision period, ω is gyro-frequency and the subscripts e and i refer to electrons and ions, respectively.

For the pulsed inductive accelerator this time would be about $0.5\mu s$, which is a little less than the stroke period of the accelerator. This would appear to indicate that ion current should be expected in a typical impulsive accelerator. However, it is emphasized that Spitzer's calculation is for contant E and B fields; the field changes associated with the subsequent current are neglected. This means that a current is permitted to occur with $\nabla XH = 0$ and that a jxB force exists with no magnetic pressure gradient. This is far from true in an impulsive accelerator where all of the magnetic field arises from the current. For this reason, Spitzer's

Presented as Paper 71-607 at the AIAA 4th Fluid and Plasma Dynamics Conference, Palo Alto, Calif., June 21–23, 1971; submitted June 21, 1971; revision received September 20, 1971. P. Weber was responsible for the construction and setup of all diagnostic and test equipment. His skillful work is gratefully acknowledged. This research was sponsored by the Air Force Office of Scientific Research (AFOSR), Air Force Systems Command, U.S. Air Force, under AFOSR Contract F44620-68-C-0042.

Index category: Electric and Advanced Space Propulsion.

* Electric Propulsion Staff. Member AIAA.

† Professor of Physics.

indication of ion current is not applicable to the impulsive accelerator.

The present work was undertaken in an effort to remove the ambiguity still surrounding the behavior of the pulsed inductive accelerator and to relate its operation to that of the electrode impulsive devices.

Approach

Miniature coils are used to measure radial and axial magnetic field components, floating electrode pairs are used for both θ and axial components of electric field; current density is measured both by computing the curl of the magnetic field and by using a miniature Rogowsky loop, whereas electron density is determined from scattered laser light. All of these techniques are well known and in common use.

In our earlier work with a 10-cm-diam accelerator, we adopted a radial station midway between the inner and outer coil radii to characterize the current sheet. This has left open the question whether a complex radial structure, for example counter rotating inner and outer cells of plasma, could occur. To remove objections of this nature and show that properties at a particular radius are really representative, all of the axial probe surveys were made at several radii. Laser scattering measurements of electron density were made at one radial position only.

These measurements are sufficient to determine V_θ through the use of the complete Ohm's Law. A cylindrical coordinate system is used where z is the direction of axial motion, r is radius and θ is azimuthal angle taken positive clockwise looking in the z direction.

The general Ohm's Law relation is

$$\mathbf{E}+\mathbf{V}\times\mathbf{B}+\nabla P_e-\mathbf{j}x\mathbf{B}/en_e-\eta\mathbf{j}=0 \qquad (2)$$

where a $\partial j/\partial t$ term has been omitted which is unimportant for periods long compared to the plasma period. *MKS* units are used throughout this paper. The z component of Eq. (2) is

$$V_\theta = E_z/B_r+j_\theta/en_e+(1/en_eB_r)\partial P_e/\partial z$$

With the assumption that

$$n_e\partial T_e/\partial z \ll T_e\partial n_e/\partial z$$

the V_θ equation can be written

$$V_\theta = E_z/B_r+j_\theta/en_e+(T_e/B_rn_e)\partial n_e/\partial z \qquad (3)$$

Here, e is electron charge, T_e is electron temperature in electron volts, n_e is electron density, V is mass velocity (essentially ion velocity), j is current density, B and E are magnetic and electric fields and r, z and θ are the cylindrical coordinates. A measurement of electron temperature and density has shown that the above inequality is reasonable for conditions similar to those of the present experiment.[9]

The θ component of Eq. (2) can be written

$$E_\theta+V_zB_r=\eta j_\theta \qquad (4)$$

Since the fields and current density are the only measured quantities, both η and V_z are inferred variables. Consequently, its usefulness is limited to regions where V_z is known, e.g., in front of the sheet where $V_z=0$ and the region where the accelerated nass is moving at a nearly constant velocity. For such regions, the resistivity can be found and the electron temperature calculated from Spitzer's relation for Coulomb collisions in a fully ionized plasma with a transverse magnetic field.

$$\eta = 1.031\times10^{-3}/T_e^{3/2} \qquad (5)$$

Diagnostics

Axial and radial magnetic field components were mapped with conventional glass-enclosed loop probes of 1 mm window diam and 2 mm jacket diam; their frequency response was measured to be flat to at least 7 Mhz. For very fast B_r transients, a single turn open rectangular loop ($\Delta Z = 1$ mm, $r\Delta\theta = 1$ cm) was used. Its L/R rise time into 50 ohms was 2×10^{-10}s. The Rogowsky coil used for direct j_θ current density mapping was given a rectangular shape ($\Delta Z = 6$ mm, $\Delta r = 13$ mm). Its rise time into 50 ohms was 6×10^{-8} sec; although this response was slower than that of the probes, the limitation was not deemed serious, since most of the signals did not require anything faster.

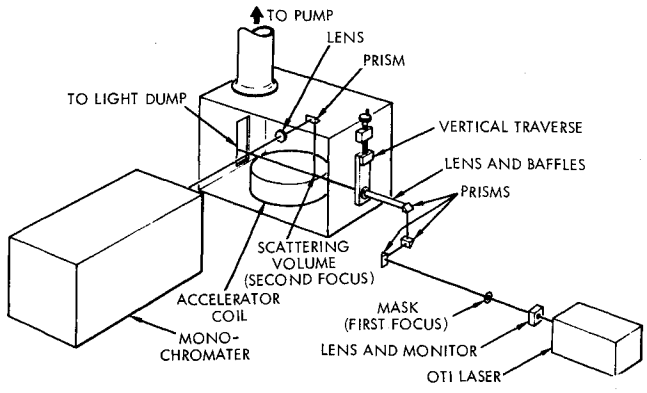

Fig. 1 Geometry of laser scattering experiment.

Electric field measurements were made by the standard differential floating-probe technique.[7] Since E_θ is not a function of θ, the electrode separation along this coordinate was made relatively large (1.67 cm) in order to improve signal-to-noise ratio. For E_Z measurements, the separation in Z was 3 mm.

All probes were mounted on a carriage that allowed traversal in r and Z over the entire region of interest.

Measurements of the electron density distribution were made by scattering of laser light. The layout is shown in Fig. 1. The beam from an OTI model 130 laser (approximately 1 joule in 20 nanosec) was passed through a set of three right-angle reflecting prisms which rotated the polarization into the horizontal direction so that the light scattered along Z into the detector would be maximal, and also allowed a scanning of the beam in the Z-direction while the laser remained stationary. The incident beam entered the system along r, and was focused to a diameter of 1 mm at the observed scattering position which was always at a radius of 7 cm. A 1.5 cm length of the beam was imaged, with unity magnification, upon the input slit of the monochromator.

The original intention had been to determine both n_e and T_e through analysis of the spectral profile of the "electron feature."[10]

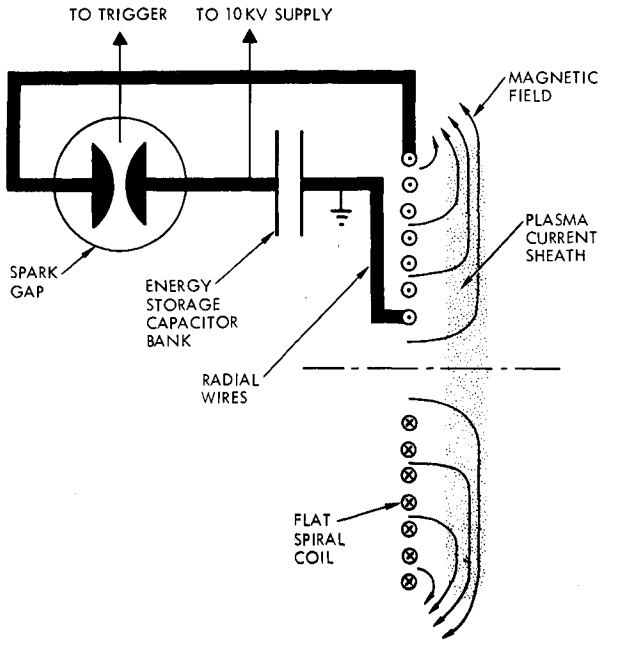

Fig. 2 Schematic diagram of accelerator circuit.

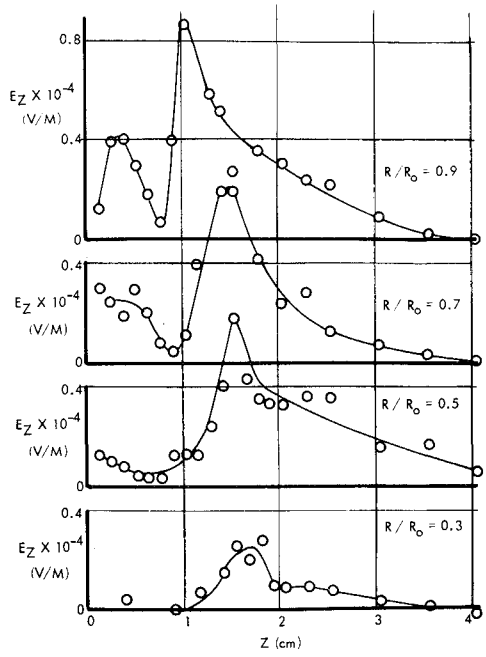

Fig. 3 Axial distribution of electric field due to charge separation for four radial positions.

However, upon examination of the scattered spectrum, it became evident that within the signal-to-noise capabilities of the system, no electron spectrum could be detected. The entire detectable scattering was within 5 Å of the laser wavelength, a characteristic of scattering from ion-related density fluctuations. Since both the laser and monochromator had bandwidths too great to allow resolution of the "ion feature" spectrum, it was only possible to determine total density through a measurement of relative scattered intensity as compared to Rayleigh scattering from neutral Argon.

Description of Accelerator

The circuit is shown in Fig. 2. The capacitor bank consisted of nine 0.44 μf capacitors operated at 12 kv with a stored energy of 285 joules. The accelerator coil was a flat spiral consisting of nine conductors, each making a two-turn spiral from a 20 cm O.D. to a 6 cm I.D. The spiral was machined out of a 3 mm thick brass plate. The conductors were 3 mm wide with a gap of $1\frac{1}{2}$ mm between adjacent conductors. The inductance of the circuit varied from a minimum of 64×10^{-9} henrys, with a metal plate laid against the Mylar cover, to a maximum of 452×10^{-9} henrys with the plate removed.

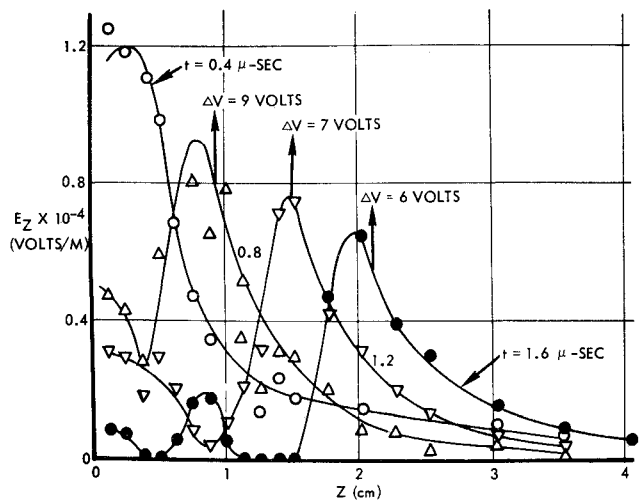

Fig. 4 Axial distribution of electric field due to charge separation at 0.4, 0.8, 1.2 and 1.6 μ-sec.

Results

Probe Data

Probe surveys of radial and axial magnetic fields, axial electric field, azimuthal electric field and azimuthal current density were taken at intervals of 1 mm in the axial direction for a constant radius and at test conditions of 12 kv and 500 millitorr of argon. The axial scans were repeated at radial intervals of $2\frac{1}{2}$ mm for magnetic field data, at 5 mm intervals for electric field data and at 1 cm intervals for azimuthal current density. The uniformity of the current sheet over the coil face is illustrated by the electric field plot in Fig. 3, while the propagation of the sheet can be seen in Fig. 4.

Electron Density

It is customary to obtain an estimate of electron density by using Eq. (3) with the assumption that the electron pressure gradient is unimportant and the ions are not carrying current ($V_\theta = 0$). With these qualifications, Eq. (3) becomes

$$n_e = -j_\theta B_r / eE_z \tag{6}$$

and the electron density is determined in terms of three probe measurements alone, or two, in the event that j_θ is derived from $B_r(r, z)$, In regions of large j_θ and low E_z the inferred density becomes too large to be plausible and the simplifying assumptions must be re-examined.

As long as E_z remains positive it is conceivable that the V_θ term should be included. As mentioned earlier this means angular momentum appears without a corresponding torque mechanism, for the inductive geometry. In the present experiments, however, the fact that E_z becomes negative after 1.6 microseconds makes it even more unlikely that ion current is the proper interpretation.

A more plausible position is to assert that V_θ is zero and include the density gradient term from Eq. (3). The result is then

$$n_e = -j_\theta B_r / eE_z - (T_e/E_z)\,\partial n_e/\partial z \tag{7}$$

Toward the front of the current sheet, forward of the station where n_e is a maximum, E_z is positive and large, the density gradient is negative and the term on the right contributes a positive increment to the calculated density. On the coil side of the maximum density location the density gradient term makes a negative contribution to the density as long as E_z is positive. This prevents the density calculated by Eq. (6) from becoming extremely large as E_z approaches zero.

The electron density for a fixed time can be calculated by numerical integration by using the following rearrangement of Eq. (7)

$$dn_e/dz = -(1/T_e)(n_e E_z + j_\theta B_r/e) \tag{8}$$

Equation (8) provides a plausible interpretation of the sharp drop in E_z to values near zero while the current density remains large. Both the large electron density and density gradient contribute to the effect. However, the density calculated in this way is effectively an "answer coefficient" that forces a certain consistency on the probe data. An independent check of electron density was therefore needed to verify the general features of the calculated distribution.

Electron Density Measurement

Figure 5 shows a typical measurement of laser light scattered at a 90° angle by the electrons. The randomness shown is representative. A beam monitor was used to allow the measurements to be normalized to a constant laser beam intensity so that variations in laser output did not contribute to the scatter.

The density distribution measured at 1.2 μs is shown as the dashed line in Fig. 6. The total number of electrons represented by this distribution is 1.9 times greater than the number of atoms at the fill density of 1.6×10^{16} per cc. This result agrees with a similar measrement at the second half-cycle discharge in a nitron theta pinch where the ratio of electrons to the original neutrals was 2.2.[9]

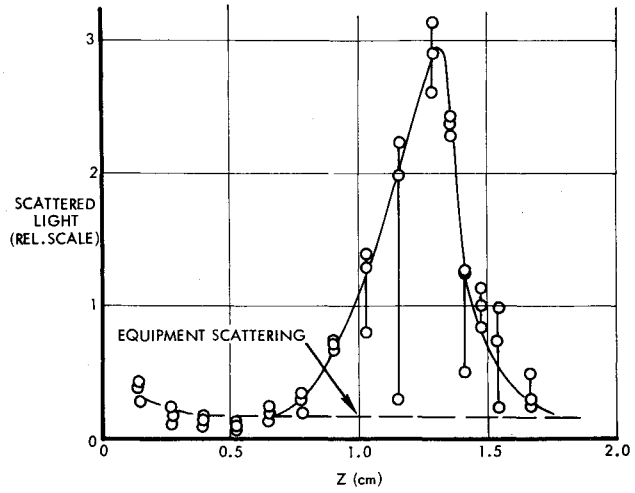

Fig. 5 Typical axial distribution of laser light scattered by electrons ($t = 1.32$ μ-sec, $R/R_o = 0.7$).

Current Sheet Structure

An overlay of the various measurments at 1.2 μs is shown in Fig. 7. The accumulated plasma is in a layer that is only 4 mm thick, at half amplitude. The electric field is large ahead of the mass layer only, whereas the current density is the largest feature of the sheet, extending over both the mass layer and the high E_z region.

A consideration of the forces in these various regions shows why these relations must exist. The forward part of the sheet ionizes and accelerates the gas up to the speed of the mass layer. The $j_\theta B_r$ force in this region combines with the electron pressure gradient force to produce a large E_z force which accelerates the ions. On the coil side of the mass layer the $j_\theta B_r$ force works against the pressure force of the electrons to prevent them from expanding the mass layer back toward the coil.

Shock Feature

Early in the probe investigation it was noticed that a well-defined positive jump occurred in the E_z data which was quickly followed by an abrupt negative jump, the interval between jumps corresponding to the transit time of the mass layer moving at 1.55 cm per μs across the probe tips spaced at 3 mm.

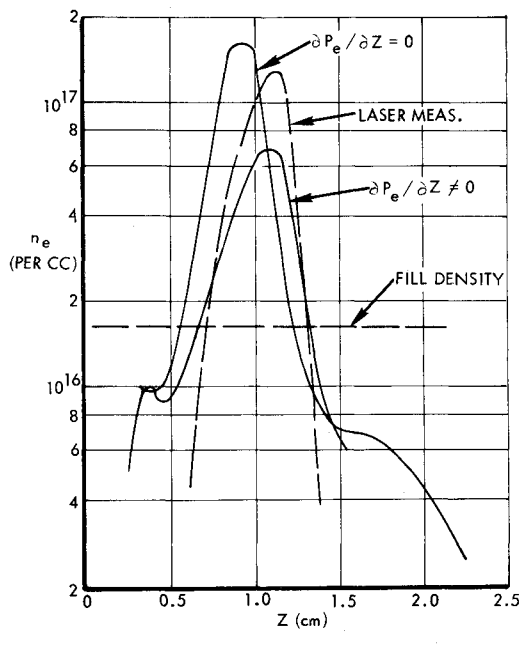

Fig. 6 Comparison of electron density distributions from light scattering and probe data.

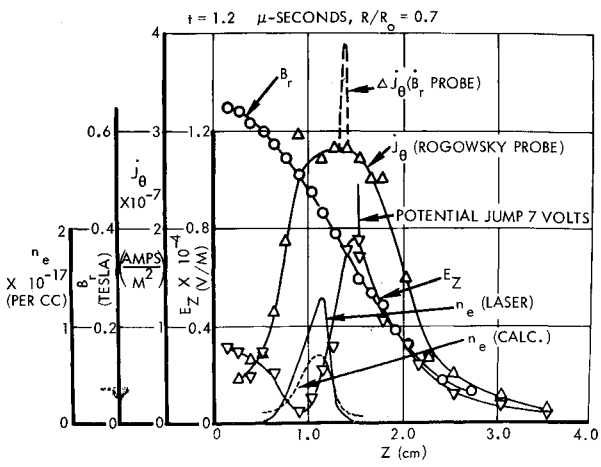

Fig. 7 Characteristic properties of impulsive current sheet ($t = 1.2$ μ-sec, $R/R_o = 0.7$).

Evidently the current sheet contains an abrupt step in floating potential which rises faster than the scope rise time. A corresponding jump had not been seen with the 5-turn glass jacketed B_r probe, but it was detected with the fast response 1-turn rectangular probe described earlier. The rise in B_r appears to occur in about 5 nsec. Since the disturbance travels at 1.55 cm per μs, this gives a thickness of the front of about 0.08 mm. Even this is an upper limit since the front edge of the rectangular probe was not aligned more accurately than this with the directon of the coil face.

The jump in j_θ is obtained from the $\dot{B}_r$ trace using the known velocity of the disturbance V and the Curl-H equation with $B_z = 0$. Thus,

$$\Delta j_\theta = (1/\mu V)\Delta \dot{B}_r$$

The magnitude and location of the jump is shown in Fig. 7 but the shape is not accurately represented.

It seems certain that a shock-like discontinuity of substantial intensity is embedded in the current sheet. It is not a precursor event since it is located near the maxima of j_θ and E_z and at the leading edge of the mass layer where E_z abruptly decreases. It is an important feature of the impulsive current sheet that has not been observed before, so far as we know. Further investigation will be needed to determine whether this shock is possibly of "collisionless" character.

We estimate the collisionless skin depth c/ω_{pe} to be about 10^{-3} cm, and the "resistive shock" thickness to be

$$\delta_{res} \equiv (c/\omega_{pe})^2 \nu_{eff}/V_z \simeq 1 \text{ cm}$$

where ω_{pe} is the electron plasma frequency, and ν_{eff} is the electron-ion collision frequency as deduced from plasma resistivity and the Spitzer resistivity formula. Since the discontinuity is observed to be not thicker than 0.1 mm, the present observations tend to favor a collisionless shock interpretation.

Conclusions

The pulsed inductive accelerator carries a pure j_θ current in a thin sheet extending over most of the coil area. Conditions are fairly constant over the outer half of the coil diameter. A consistent interpretation of the probe data and laser measurement of electron density has been made by including the electron pressure gradient force.The forward region of the current sheet contains a large electron current density which produces a strong charge separation electric field to accelerate the ions. The accelerated plasma collects in a thin mass layer (4 mm thick) near the center of the current sheet. The large negative electron pressure gradient at the leading edge of this layer increases the axial electric field, bringing the ions up to the sheet speed as they join the high-density mass layer. At the rear of the mass layer, the electron pressure gradient becomes suddenly large and positive, counteracting the $j_\theta B_r$ force on the electrons and virtually eliminating the

axial electric field. In this region the $j_\theta B_r$ force serves to hold the mass layer together but little mass acceleration is possible.

The current is carried by electrons only. The E_θ force on the ions is balanced by the resistivity force of the current carrying electrons so that no θ velocity develops. The E_z force is adequate to account for the axial motion with no requirement for an additional $V_\theta B_r$ force. The electron density distribution calculated by numerical integration of the general Ohm's Law relation, containing the electron density gradient, is consistent with the laser measured distribution and provides a consistent interpretation of all of the probe data.

References

[1] Lovberg, R. H., "Acceleration of Plasma by Displacement Currents Resulting from Ionization," *Proceedings of the VI International Conference on Ionization Phenomena in Gases*, Vol. IV, Faculté des Science de Paris, 1963, pp. 235–239.

[2] Dailey, C. L., "Plasma Properties in an Inductive Pulsed Plasma Accelerator," AIAA Paper 65-637, Evanston, Ill., 1965.

[3] Bodin, H. A. B., et al., "The Influence of Trapped Field on the Characteristics of a Magnetically Compressed Plasma (Thetatron)," *Nuclear Fusion*, 1962 Supplement, Pt. 2, pp. 521–532.

[4] Bodin, H. A. B. and Newton, A. A., "Rotational Instability in the Theta Pinch," *The Physics of Fluids*, Vol. 6, No. 9, Sept. 1963, pp. 1338–1345.

[5] Dailey, C. L., "Plasma Rotation in a Pulsed Inductive Accelerator," *Proceedings of the XVII Astronautical Congress*, PWN-Polish Scientific Publishers, Vol. III, 1966, pp. 253–260.

[6] Lovberg, R. H., "Investigation of Current Sheet Microstructure," AIAA Paper 65-335, San Francisco, Calif., 1965.

[7] Dailey, C. L., "Investigation of Plasma Rotation in a Pulsed Inductive Accelerator," *AIAA Journal*, Vol. 7, No. 1, Jan. 1969, pp. 13–19.

[8] Spitzer, L., *Physics of Fully Ionized Gases*, Interscience, New York, 1956.

[9] Siemon, R. E., "Current Sheet Structure in a Low Energy Theta Pinch," Ph.D. thesis, 1969, Univ. of California, San Diego.

[10] Salpeter, E. E., "Electron Density Fluctuation in a Plasma," *Physical Review*, Vol. 120, No. 5, 1960, pp. 528–535.

FEBRUARY 1972 AIAA JOURNAL VOL. 10, NO. 2

Roll Resonance and Passive Roll Control of Magnetically Stabilized Satellites

R. W. KAMMÜLLER*
European Space Research and Technology Centre, Noordwijk, Holland

The resonant roll solutions of the magnetically stabilized satellite are investigated using a variational approach. The variational problem is solved by the numerical method of Ritz. A parameter study is made for the case of the satellite ESRO I. The basic properties of the different classes of solution are discussed. Emphasis is laid on the class of rotational solutions. A policy for the optimal selection of the inertial parameters is defined. The optimized spacecraft sustains stable rotational roll motions. The policy allows control of the class of roll motions in a passive way. The results of the analysis generally agree with observed ESRO I flight data.

1. Introduction

THE type of satellite considered here belongs to the class of spacecraft oriented by magnetic means.[1] The control principle as illustrated in Fig. 1, represents a passive one-axis control. A simple permanent magnet, fixed rigidly to the structure of the spacecraft, is used to align the reference axis (Z axis) of the satellite to the local direction of the Earth magnetic field. A number of ferromagnetic rods placed normal to the reference axis are applied to damp the libration motions of the satellite. This type of control is usually chosen to orient small scientific satellites designed for auroral and ionospheric studies in near-polar orbits. Owing to the dipole character of the geomagnetic field, the orbiting spacecraft is forced to perform a "head-over-heels" motion around its lateral axis. This motion shall later be called the pitch motion whereas the motion around the reference axis shall be denoted as the roll motion of the spacecraft. In a previous paper the residual roll motion for the general non-symmetrical rigid body has been analyzed and the appearance of resonant roll solutions has been predicted.[2] It could be shown that the roll resonance effect is parametrically excited by the non-uniform components of the pitch motion, the mechanism for the exchange of energy between pitch and roll motion being provided by inertial crosscoupling. By use of a perturbation method the existence of a large variety of harmonic and subharmonic solutions of the oscillatory type could be proven.

The present paper extends the investigations to the class of

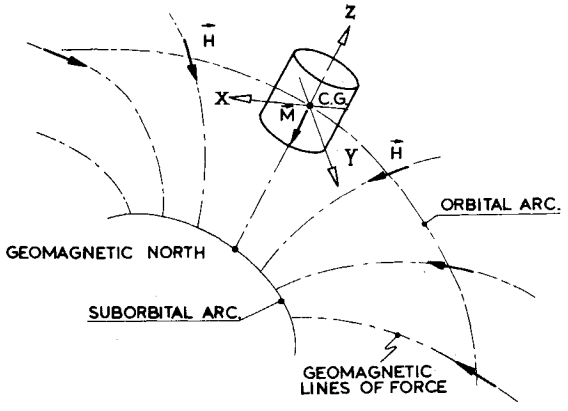

Fig. 1 Orientation of the magnetically stabilized satellite above the northern polar region, M—magnetic dipole moment of satellite, H—local gradient of the geomagnetic field.

Received March 1, 1971; revision received August 12, 1971. Presented at the XXIst International Astronautical Congress, Constance, Germany, October 1970, in abbreviate form.

Index category: Spacecraft Attitude Dynamics and Control.

* Research Engineer, Satellite and Sounding Rockets Department.